Spark plasma versus conventional sintering in the electrical properties of Nasicon-type materials

M. Pérez-Estébanez[a, d, *]

martaestebanez@quim.ucm.es

J. Isasi-Marín[a]

A. Rivera-Calzada[b]

C. León[b]

M. Nygren[c]

[a]Dep. Química Inorgánica I, Universidad Complutense de Madrid, Ciudad Universitaria s/n, 28040 Madrid Spain

[b]Dep. Física Aplicada III, Universidad Complutense de Madrid, Ciudad Universitaria s/n, 28040 Madrid Spain

[c]Dep. Materials and Environmental Chemistry, Arrhenius Lab. Stockholm University, S-106 9 Stockholm Sweden

[d]Centre Excellence Telč, Institute of Theoretical and Applied Mechanics, Batelovská 485, 58856 Telč Czech Republic

*Corresponding author. Centre Excellence Telč, Institute of Theoretical and Applied Mechanics, Batelovská 485, 58856 Telč Czech Republic.

Abstract

$Li_{1+x}M_xTi_{2-x}(PO_4)_3$ powders with x = 0 and 0.3 and M = Al, Cr and Fe have been sintered by conventional sintering (CS) and Spark Plasma Sintering (SPS), and the electrical properties have been compared. The use of SPS allows preparing samples with higher density at lower temperature and shorter time than the CS, avoiding segregation of secondary phases and with reduced crystallite size. The introduction of aluminum, chromium and iron in the $LiTi_2(PO_4)_3$ (LTP) clearly enhances ionic conductivity even if the samples have similar densities. Despite the different level of density reached with CS and SPS, the activation energies of dc and grain boundary contributions are very similar and the differences in ionic conductivity are determined by pre-exponential factors. The samples produced by SPS showed a well-defined grain boundary meaning a more homogenous electrical contact.

Keywords: Electrode materials; Sintering; Ionic conduction

1 Introduction

Solid lithium conductors have been attracting a great interest during the last decades due to their potential applications in lithium batteries, sensors and fuel cells [1–9]. Nasicon-type materials were first discovered as three-dimensional ionic conductors and since then many studies have focused on the development of Nasicon materials with optimized properties. $LiTi_2(PO_4)_3$ (LTP) and its derivatives are among the best candidates [10–19]. As it has been repeatedly described, the electrical properties of LTP are highly improved by the substitution of Ti^{4+} with a trivalent metal giving rise to compounds of formula $Li_{1+x}M_xTi_{2-x}(PO_4)_3$ [10,20–22]. There are two reasons for the improvement of the ionic conductivity: the increase in the concentration of carriers (Li^+) and the enhanced density of the powders. In a previous work, we have demonstrated that the concentration of carriers is strongly affecting the ionic conductivity in the way that the displacement of ions from the M1 position to the M2′, gives rise to a higher disorder of ions within the structure [23]. However, apart from the composition, the ionic conductivity of Nasicon materials has also a strong dependence on their density [13,24]. Traditionally, two methods have been used to increase the density of materials: the cold sintering and the melting of the material with a subsequent quenching. As it has been proved, none of these methods succeeded in the fully densification of LTP phases [25,26]. Nasicon compounds are well known to be difficult to densify by the traditional techniques (conventional sintering or hot press) [27].

The Spark Plasma Sintering (SPS) is a pressure assisted sintering method consisting in the application of a pulsed DC current along with uniaxial pressure. SPS allows a faster densification than the conventional sintering methods at lower temperature, giving rise to higher density, smaller grain size, clearer grain boundaries as well as other attractive properties [28]. The critical temperature above which the grain growth rate becomes appreciable is largely determined by the properties of the powder precursors, e. g. their particle size, reactivity, degree of agglomeration, etc., but also by the applied heating rate and pressure [29]. In order to prepare dense samples with a very limited grain growth, it is necessary to

map up the sintering parameters [30]. SPS is nowadays attracting the attention of many researches with the aim to obtain all-solid-state-batteries [31–34]. However, until now only a few papers reporting the SPS of Nasicon materials have been published [35]. $LiTi_2(PO_4)_3$ obtained by hydrothermal synthesis was sintered by SPS at 1200 °C, but only the 81% of the theoretical density was achieved [36]. Later on, the SPS of the same compound obtained by solid state reaction was reported and, on the same sintering conditions, the 95% of the theoretical density was achieved [37]. Al-substituted LTP has been sintered by SPS and fully dense materials were obtained [38–40]. Other Nasicon materials, such as $LiHf_2(PO_4)_3$ and $Na_{1+x}Zr_2Si_xP_{3-x}O_{12}$, have been successfully sintered using SPS [41,42]. Nevertheless, to the best of our knowledge, there is no paper reporting the systematically study of M^{3+}-substituted LTP materials sintered by SPS.

In this work, Spark Plasma Sintering has been used in order to obtain full dense pellets with composition $Li_{1+x}M_xTi_{2-x}(PO_4)_3$. The sintering parameters were optimized to obtain the highest density and avoid grain growth. Four different materials were densified: $LiTi_2(PO_4)_3$ (LTP), $Li_{1.3}Al_{0.3}Ti_{1.7}(PO_4)_3$ (LATP), $Li_{1.3}Cr_{0.3}Ti_{1.7}(PO_4)_3$ (LCTP) and $Li_{1.3}Fe_{0.3}Ti_{1.7}(PO_4)_3$ (LFTP). With the aim of studying the differences in the sintering behaviour of $LiTi_2(PO_4)_3$ when adding Al, Cr and Fe, the substitution degree in LTP was fixed. The electrical properties of the fully dense materials are compared with samples with low density produced by conventional sintering that were already reported by us [23], in order to determine the effect of the density on the ionic conductivity of these compounds.

2 Material and methods

2.1 Sample preparation

$Li_{1+x}M_xTi_{2-x}(PO_4)_3$ samples with x = 0, 0.3 and M = Al, Cr and Fe were prepared by the Pechini sol–gel method following the procedure reported elsewhere [43]. The obtained powders were then compressed and densified by conventional sintering (CS) and spark plasma sintering (SPS). CS treatment consisted on the cold pressing of the powder into pellets of 13 mm diameter and 1 mm thickness using a uniaxial pressure of 150 MPa and a subsequent sintering treatment at 1000 °C for 12 h. SPS experiments were carried out in an SPS unit Dr. Sinter 2050 (SPS Syntex Inc., Japan). Before SPS treatment, samples were mechanically milled in ethanol at 100 rpm during 10 min for homogenization. After drying, powders were loaded in a cylindrical graphite die with 12 mm of inner diameter and enclosed by graphite papers. In order to isolate the sample from the electrical current, powders of Al_2O_3 were placed both on the bottom and the top of the sample in a way that a nonconductive layer of 1.5 mm thickness was performed. The die was heated by allowing a pulsed direct current to pass through it with pulses of 3.3 ms and a pulse sequence of 12 pulses On: 2 pulses Off. The On–Off voltage creates spark discharge, generating high temperature and Joule heating between particles [44]. The maximum voltage and current were 3.5 V and 635 A respectively. The temperature was measured with a thermocouple inserted into the graphite die. The set-up is provided with a dilatometer for recording the shrinkage. Linear shrinkage, ΔL, temperature, pressure, average voltage and current are recorded during the process. The ΔL-values were corrected for the contribution related to the expansion of the graphite die set and the Al_2O_3 layers through a zero-curve. In a first set of experiments, the kinetic window within which it is possible to obtain dense ceramics and simultaneously reduce grain growth, were defined using standard conditions, meaning a constant heating rate of 50 °C/min and a pressure of 75 MPa. The onset temperature (T_0) is defined as the temperature at which shrinkage starts. The temperature at which ΔL is constant, that is, the sample has achieved its final density, is known as final temperature (T_f). During the experiments, the onset and final temperatures of densification were determined. When T_f was reached, the pressure was released and sample was cooled down. After sintering, SPS samples were polished to remove the graphite paper and annealed in air at 700 °C for few hours.

2.2 Characterization

The density of the samples was determined by the Archimedes method using water as the immersion fluid.

XRPD patterns were collected on a Philips X'Pert PRO instrument using CuKα_1 radiation,(45 kV, 40 mA) with a PW 3050/00 goniometer in a Bragg–Bretano configuration and a Germanium X´ Celerator detector. A step scan of 0.033° (2θ) in the range 10–120° and a counting time of 350 s were employed. Quantitative phase analysis was carried out by means of the Rietveld method implemented in the Fullprof software [45].

Microstructural studies were made by FEG–SEM observations of the fracture surface of the pellets using secondary electrons. A JEOL JSM 6335F microscope was used working at 40 kV accelerating voltage. The mean grain size has been obtained from the images measuring at least 100 grains.

The electrical properties were analyzed by impedance spectroscopy. Measurements were carried out in a BDS80 from Novocontrol, in the frequency range 10^{-2}–10^7 Hz at selected temperatures between −150 and 250 °C with the integrated Quatro temperature control system with accuracy of ±0.1 K. Electrical contacts were made with silver paint and an inert atmosphere was ensured by measuring the samples under N_2 flow.

3 Results

3.1 Densification by SPS

Table 1 shows the observed T_0, T_f and final density for each sample, together with the experimental parameters used in the standard experiments. Density values of samples processed by CS are also included for comparison.

Table 1 Sintering parameters of standard experiments, T_0, T_f and final density values. The values of density of samples obtained by CS is added for comparison.

Sample	Heating rate	T_0	T_f	Holding time	Pressure	Density SPS	Density CS

LTP	50 °C/min	760 °C	950 °C	5 min	75 Mpa	90%	60%
LATP	50 °C/min	760 °C	950 °C	3 min	75 Mpa	98%	71%
LCTP	50 °C/min	720 °C	850 °C	5 min	75 Mpa	86%	51%
LFTP	50 °C/min	540 °C	700 °C	0 min	75 Mpa	95%	65%

As it can be observed, the SPS gives rise to high density pellets in a shorter time than the CS. Using both techniques, the highest values were reached in the LATP samples and the lowest in the LTP and LCTP. Values of at least 85% of the theoretical density were obtained using SPS in contrast with the poorly densified samples obtained by CS. Once activated, the densification occurs very fast, within less than 10 min, and in a very narrow temperature interval. The onset of shrinkage starts at 720–760 °C for the LPT, LATP and LCTP samples and at 540 °C for the LFTP. The onset of shrinkage is generally known as the starting point of the grain sliding mechanism, where the open pore channels start to shrink [46]. Fig. 1 shows the linear shrinkage rate plotted versus time observed during SPS. The linear shrinkage rate is defined as $d(-\Delta L/L_0)/dt$, with L_o being the thickness of the green ~~(in the web version)~~ ~~(Green body is called to the simple before sintering, is not any color in the Figures, so the comment (in the web versión is not correct))~~ body at room temperature under the appropriate pressure. The occurrence of a maximum linear shrinkage rate indicates a change of densification mechanism from grain sliding one to a controlled diffusion grain growth mechanism [46]. The sample LFTP shows the highest shrinkage rate, which is actually achieved at lower temperature. LATP and LCTP show similar curves, but a broader curve is obtained in the LTP sample, meaning a slower sintering kinetics.

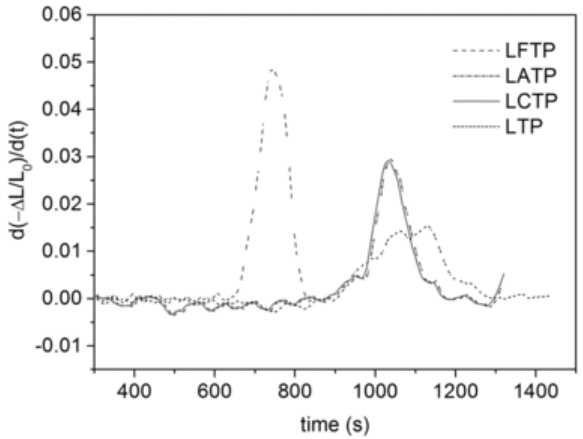

Fig. 1 Linear shrinkage rate plotted versus time for the different samples in conditions shown in Table 1.

Once the kinetic sintering window was obtained, several conditions were tested to optimize the sintering process in order to achieve the highest density with a reduced grain growth. Samples were heated to the temperatures of the maximum shrinkage rate according to the sintering curves recorded in the standard experiments, and the best results were obtained using a pressure of 90 MPa. Table 2 contains the sintering parameters and final densities of this second set of experiments. The use of a higher pressure decreases the onset temperature more significantly in samples LTP and LATP, but the temperature interval of sintering becomes broader (230 and 260 °C respectively). In the sample LCTP, the onset temperature was decreased in 35 °C but the final temperature was constant. Finally, for the LFTP sample, although the onset temperature was only slightly decreased, the sintering procedure finishes at a temperature 100 °C lower, meaning a faster sintering lasting less than 10 min, as it can be seen in the sintering curves (Fig. 2). In the sintering curves the percentage of the theoretical density versus time is plotted. Also the heating ramps are included. As it can be noticed, the sintering time for the LFTP sample is less than half of the time needed for the other samples.

Table 2 Sintering parameters of second series of experiments, T_0, T_f and final density values.

Sample	Heating rate	T_0	T_f	Holding time	Pressure	Density SPS
LTP	50 °C/min	670 °C	900 °C	2 min	90 MPa	91%
LATP	50 °C/min	640 °C	900 °C	0 min	90 MPa	99%
LCTP	50 °C/min	685 °C	850 °C	5 min	90 MPa	89%

LFTP	100 °C/min	520 °C	600 °C	3 min	90 MPa	94%

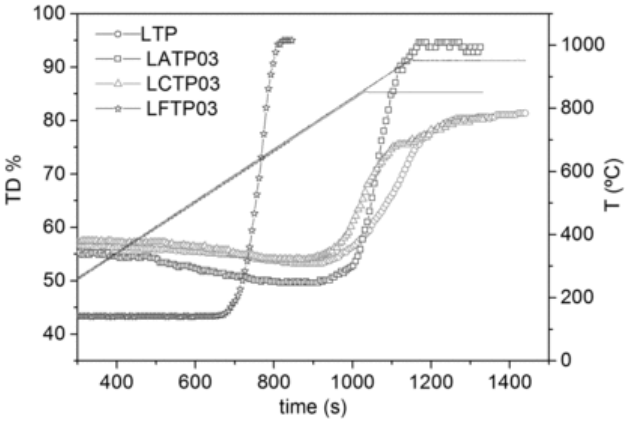

Fig. 2 Shrinkage curves of samples sintered with a pressure of 90 MPa in conditions shown in Table 2.

3.2 Characterization

XRPD patterns were collected at room temperature for all samples. A zoom in the range 15–40° in 2θ is shown in Fig. 3. All samples prepared by SPS conserve the Nasicon-type structure with rhombohedral symmetry (S.G. $R\bar{3}c$) and no evidence of impurities was found. On the other hand, in the CS samples of composition LCTP and LFPT, new maxima due to TiO_2-rutile can be observed after sintering. The amount of rutile has been quantified by Rietveld refinement and corresponds to a 6.2(1) and 17.1(3) of wt% in LCTP and LFTP respectively. Sample of composition LATP shows small maxima corresponding to a new phase with NASICON structure, but have different cell parameters than the original one (a = 8.5032(1) Å and c = 20.8339(3) Å in the majority phase, and a = 8.4815(7) Å and c = 21.6251(9) Å in the minority phase); in a way that the *c/a* ratio is increased from 2.44 to 2.55. This fact can be related with a bigger size of the M1 cavity as it occurs in the $NaTi_2(PO_4)_3$ compound [10]. Some authors have suggested that the Al^{3+} ions go to the Li^+ places [47]. Anyhow, such variation in the unit cell may be a consequence of the heterogeneity in the ~~aluminium~~ aluminum substitution within the crystal structure. The mean crystallite size of the SPS samples was estimated using the Scherrer equation [48]. The obtained values are 44, 49, 56 and 67 nm for the samples LFTP, LCTP, LTP and LATP respectively. The LATP sample show the biggest crystallite size followed by LTP, which are the samples sintered at the highest temperature. The sample LFTP has the smallest crystallite size due to the lowest sintering temperature. Besides, in Fig. 3 it can be noticed that broader peaks are obtained in SPS samples compared with CS due to a smaller crystallite size. The applicability of the Scherrer formula is limited to crystallites up to 100 nm, which disallows us to apply it to the samples obtained by CS. However, from the structural point of view, the use of SPS allows to successfully prepare samples with higher density at lower temperature and shorter time avoiding segregation of secondary phases and with reduced crystallite size.

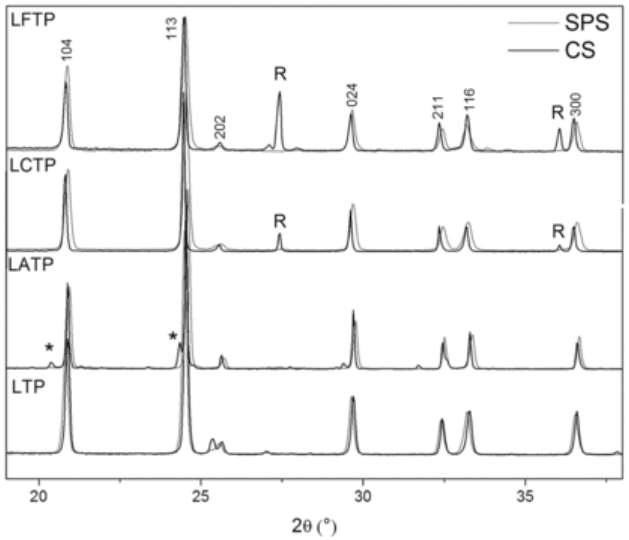

Fig. 3 XRPD patterns after SPS and CS. in the range 15–40° 2θ.

SEM micrographs of the fracture surfaces with 1500 magnification are shown in Fig. 4 (SPS) and Fig. 5 (CS). The differences in the microstructure obtained by both sintering treatment are notable. The use of SPS gives rise to samples with much higher degree of densification where grain boundaries are difficult to identify. In Fig. 4, samples showing high density can be seen with homogeneous microstructure except for LATP (Fig. 4b), which is also fairly dense but exhibited large particles embedded in a fine grained environment. The biggest grains have irregular shape and average size of 1.4 μm, and the smallest have been measured to have an average size of 680 nm and spherical shape. This bimodal microstructure is also observed in the sample LATP–CS (Fig. 5b), so it is not related to the sintering method but due to the composition. As it has been reported for different materials, abnormal grain growth may be associated with a small shift in the stoichiometry of the samples [49]. This inhomogeneity of the composition may be present in the original powders before sintering but it is noticeable by XRD only after CS most likely due to the high temperature and long sintering treatment. There has been reported recently the compositional dishomogeneity in LATP samples by Arbi et al. [50,51], a core–shell microstructure in which the shell is deficient if Al has been proposed.

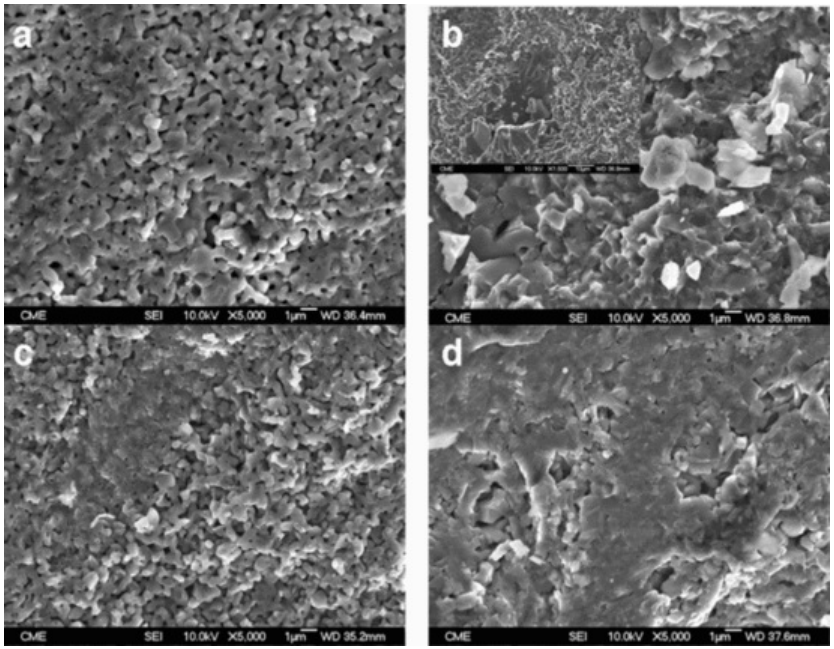

Fig. 4 SEM micrographs of samples LTP (a), LATP (b), LCTP (c) and LFTP (d) processed by SPS.

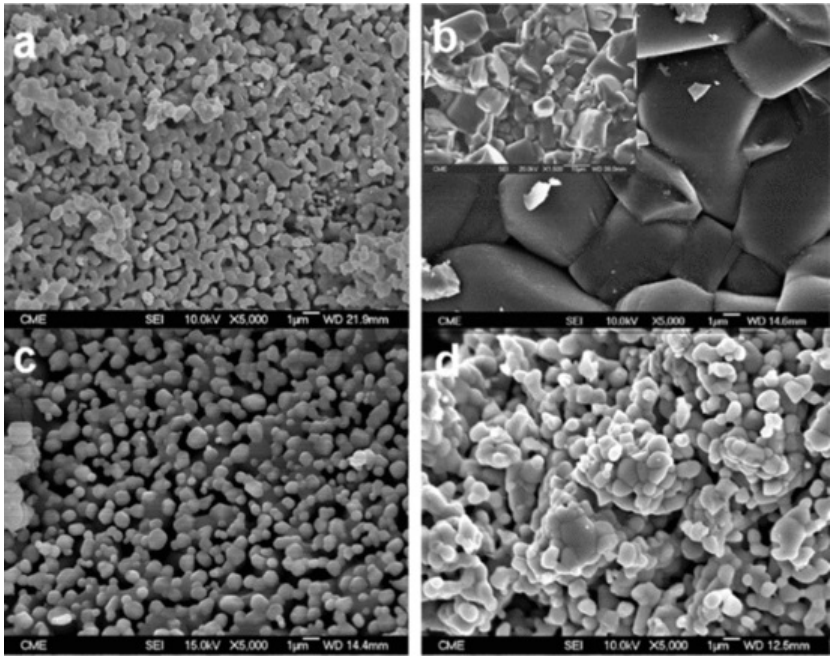

Fig. 5 SEM micrographs of samples LTP (a), LATP (b), LCTP (c) and LFTP (d) processed by CS.

LTP and LCTP are formed by spherical grains and, especially in LFTP, some subeurhedral particles are also formed. The mean grain size for samples prepared by CS and SPS are, respectively, 800 ± 250 and 400 ± 150 nm for LTP; 7500 ± 4000 and

900 ± 350 nm for LATP; 830 ± 290 and 480 ± 140 for LCTP and 1000 ± 330 and 530 ± 200 nm for LFTP. The mean grain size is smaller in the SPSed samples. Sintering takes place through densification mechanism whereas grain growth is reduced.

3.3 Impedance spectroscopy

The charge dynamics of the samples was investigated by complex impedance measurements in a wide range of frequency and temperature, which allowed us to separate the bulk dc and grain boundary mechanisms of electrical conductivity. All the samples show typical features of ionic conductors. Fig. 6 shows, as an example, the Nyquist plot, Z″ versus Z′, of LTP–SPS at −140 °C. A small semicircular arc passing through the origin can be seen in the inset, which corresponds to dc bulk conductivity. In ~~the~~ Fig. 6, the main arc which appears at lower frequencies corresponds to the grain boundary resistance and at the longest times there is a long spike due to the blocking of carriers at the electrode, the indication of the ionic character of carriers. In all the samples studied, the arc corresponding to the grain boundary conductivity is bigger than the one corresponding to the bulk, which means that the electric properties are dominated by grain boundary effects, as it is explained in the literature [38]. As a general trend, better resolution of semicircles was observed in SPS samples than that processed by CS, as a consequence of the better densification. In Fig. 7 the real part of the permittivity (ε′) versus frequency plots are presented for LATP processed by CS and SPS. A large plateau is observed in SPS sample which is not present in the CS sample. This plateau is due to the relaxation mechanisms in the grain boundaries (seen as dispersive regime in a conductivity plot). From these facts, the larger plateau and the better resolved semicircles, it can be stated that a well-defined grain boundary exist in SPS, meaning a more homogenous electrical contact.

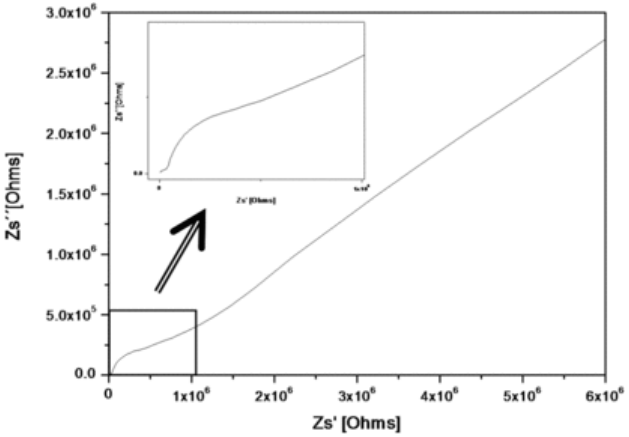

Fig. 6 Nyquist plot of LTP–SPS at −140 °C. The inset shows a zoom of the high frequencies region where the small semicircle related to bulk conductivity can be appreciated.

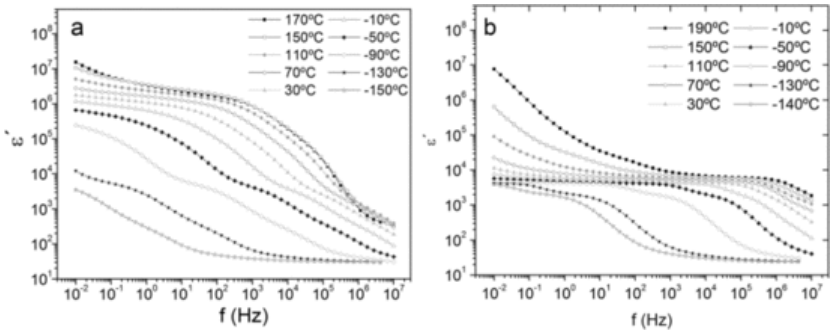

Fig. 7 Frequency dependence of the real part of the permittivity in LATP sample processed by CS (a) and SPS (b).

Bulk and grain boundary dc conductivity values were plotted in Arrhenius format and are presented in Fig. 8. Conductivity values at room temperature, activation energies and pre-exponential factors obtained from the fitting are shown in Table 3.

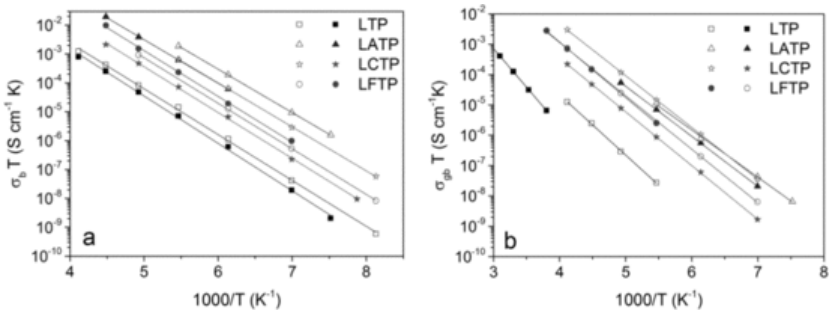

Fig. 8 Arrhenius fit of the conductivity in the bulk (a) and grain boundaries (b). Empty symbols correspond with samples processed by SPS and filled symbols by CS.

Table 3 Activation energy, pre-exponential factor and ionic conductivity at room temperature.

Sample		Bulk			Grain boundary		
		Ea (eV) ±0.01	Log σ_0 (S cm^{-1}) ±30%	σ_{RT} (S cm^{-1}) ±30%	Ea (eV) ±0.01	Log σ_0 (S cm^{-1}) ±30%	σ_{RT} (S cm^{-1}) ±30%
LTP	CS	0.33	5.8×10^3	6.0×10^{-5}	0.51	3.3×10^4	3.0×10^{-7}
	SPS	0.32	2.4×10^3	8.6×10^{-5}	0.40	1.9×10^3	1.4×10^{-6}
LATP	CS	0.30	1.7×10^5	6.2×10^{-3}	0.33	7.5×10^3	7.3×10^{-5}
	SPS	0.30	3.1×10^5	1.1×10^{-2}	0.31	3.6×10^3	6.8×10^{-5}
LCTP	CS	0.32	1.8×10^4	2.9×10^{-4}	0.35	4.4×10^3	1.6×10^{-5}
	SPS	0.30	1.4×10^5	3.6×10^{-3}	0.34	3.2×10^4	2.0×10^{-4}
LFTP	CS	0.31	1.1×10^5	2.3×10^{-3}	0.37	3.0×10^4	6.0×10^{-5}
	SPS	0.31	5.7×10^4	1.0×10^{-3}	0.35	1.3×10^4	5.3×10^{-5}

The highest values of conductivity are found in the Al-substituted samples, as expected [52,53]. Considering the different characteristics of the samples reported in the bibliography, in terms of porosity, grain size or sintering procedure, the values of conductivity and activation energy reported in Table 3 are in line with previous works [20,38,51,54]. Results shown in Table 3 reveal that the differences in the activation energy values of the bulk and grain boundaries in samples with the same composition but different density are surprisingly small. This can also be observed in Fig. 8. The activation energy in the bulk remains nearly constant with composition as it is shown in the figure by similar slopes, and the differences in conductivity are determined by pre-exponential factors. As it is the case of CS samples, the differences in the pre-exponential factors are determined by the entropy contribution, which is correlated with the disposition of Li^+ ions within the structure [23].

From the results obtained in the SPS samples, we can state that the introduction of aluminum, chromium and iron on the LTP clearly enhances ionic conductivity even if the substituted samples have similar densities as LTP. The possible causes for increased conductivity may be an increase in lithium content, a change in the bottleneck size or a change in the grain boundary character [37].

The obtained values for the bulk conductivity do not differ much with the processing technique. The LFTP and LATP samples show similar conductivity values despite the different density level reached with SPS and CS, pointing out that even if the residual porosity is high (30–35%), the connectivity between grains seems to be sufficient to ensure effective lithium transport in the samples. Similar observations are reported in zirconia samples as long as the residual porosity is <25% [55]. However, the behavior of the grain boundary conductivity changes with the different samples. LCTP and LTP samples show improved grain boundary conductivity in the SPS samples compared with CS, due to the improvement in density (89 and 91% respectively). Similar conductivity enhancement with SPS has been previously reported [37]. We highlight that the observed grain boundary conductivity in LTP–SPS ($1.45 \cdot 10^{-6}$ S cm^{-1}) is higher than values reported for cold sintering and hot pressed LTP ($4 \cdot 10^{-8}$ S cm^{-1} and $2 \cdot 10^{-7}$ S cm^{-1} respectively) [27]. Moreover the highest conductivity values ($\sigma_b = 1.1 \cdot 10^{-2}$ S cm^{-1} and $\sigma_{gb} = 8.1 \cdot 10^{-5}$ S cm^{-1}) have been found in LATP–SPS sample and are comparable to the best values of ionic conductivity reported in the literature.

4 Conclusions

In this work Spark Plasma Sintering was optimized to fabricate full dense pellets with composition $Li_{1+x}M_xTi_{2-x}(PO_4)_3$, M = Al, Fe, Cr reducing grain growth. As compared to conventional sintering, samples, prepared at lower temperatures and shorter times, avoiding segregation of secondary phases and with reduced crystallite size, have higher density. The densification process shows some differences depending on the composition. The Fe-substituted sample sinters at lower temperature than the rest. On the other hand, when inserting Al to LTP, a bimodal microstructure is developed by both sintering methods as a consequence of compositional heterogeneities in the initial powder.

In spite of the almost perfect densification of the pellets, the activation energies of dc and grain boundary contributions are very similar to the cold sintered samples, with a slight tendency to decrease in SPS samples. However the values of the dc conductivity increase with the densification, and the reported values are similar to the best found in literature, showing the SPS as a valuable tool to get fully densified ceramic samples with materials that are difficult to prepare by conventional methods.

~~Acknowledgements~~Acknowledgments

This research has been financed by the “Ministerio de Ciencia e Innovación” (MICINN, Spain) and by the “Fundación Neurociencias y Envejecimiento” (Spain) through grants MAT2010-18432 and 4153592, 4143942 respectively as well as by the MAT2013-40722-R project.

References

[1]

K. Nagata and T. Nanno, *J. Power Sources* **174**, 2007, 832–837.

[2]

X. Xu, Z. Wen, X. Yang, J. Zhang and Z. Gu, *Sol. State Ion.* **177**, 2006, 2611–2615.

[3]

J.S. Thokchom and B. Kumar, *Sol. State Ion.* **177**, 2006, 727–732.

[4]

A. Rivera, C. León, J. Santamaria, A. Varez, M.A. París and J. Sanz, *J. Non Cryst. Solids* **307**, 2002, 1024–1030.

[5]

A. Rivera, J. Santamaria, C. León, T. Blochowicz, C. Gainaru and E.A. Rossler, *App. Phys. Lett.* **82**, 2003, 2425–2427.

[6]

J. Santos-Peña, M. Cruz-Yusta, P. Soudan, S. Franger and J.J. Cuart-Pascual, *Sol. State Ion.* **177**, 2006, 2667–2672.

[7]

M. Barré, M.P. Crosnier-López, F. LeBerre, E. Suard and J.L. Fourquet, *J. Sol. State Chem.* **188**, 2007, 1011–1019.

[8]

P. Gibot, M. Casas-Cabanas, L. Laffont, S. Levasseur, P. Carlach, S. Hamelet, J.M. Tarascon and C. Masquelier, *Nat. Mater.* **7**, 2008, 741–747.

[9]

P. Knauth, *Sol. State Ion.* **180**, 2009, 911–916.

[10]

N. Anantharamulu, K. Koteswara Rao, G. Rambabu, B. Vijaya Kumar, V. Radha and M. Vithal, *J. Mat. Sci.* **46**, 2011, 2821–2837.

[11]

B. Wang, M. Greenblatt, S. Wang and S.J. Hwu, *Chem. Mater.* **5**, 1993, 23–26.

[12]

K. Arbi, M.A. Paris and J. Sanz, *J. Phys. Chem. B* **110**, 2006, 6454–6457.

[13]

J. Fu, *Solid State Ion.* **2738**, 1997, 195–200.

[14]

R. Ramaraghavulu and S. Buddhudu, *Ceram. Int.* **37**, 2011, 3651–3656.

[15]

K. Arbi, S. Mandal, J.M. Rojo and J. Sanz, *Chem. Mater.* **20**, 2002, 1091–1097.

[16]

M.A. Paris, A. Martinez-Juarez, J.M. Rojo and J. Sanz, *J. Phys. Condens. Matter* **8**, 1996, 5355–5366.

[17]

Y. Shimonishi, T. Zhang, N. Imanishi, D. Im, D.J. Lee, A. Hirano, Y. Takeda, O. Yamamoto and N. Sammes, *J. Power Sources* **196**, 2013, 5128–5132.

[18]

P. Senguttuvan, G. Rousse, M.E. Arroyo y de Dompablo, H. Vezin, J.M. Tarascon and M.R. Palacín, *J. Am. Chem. Soc.* **135**, 2013, 3897–3903.

[19]

P. Hartmann, T. Leichtweiss, M.R. Busche, M. Schneider, M. Reich, J. Sann, P. Adelhelm and J. Janek, *J. Phys. Chem. C* **177**, 2013, 21064–21074.

[20]

H. Morimoto, H. Awano, J. Terashima, Y. Shindo, S. Nakanishi, N. Ito, K. Ishikawa and S. Tobishima, *J. Power Sources* **240**, 2013, 636–643.

[21]

M. Sughama and U.V. Varadaraju, *Solid State Ion.* **95**, 1997, 201–205.

[22]

S.D. Jackman and R.A. Culter, *J. Power Sources* **230**, 2013, 251–260.

[23]

M. Pérez-Estébanez, J. Isasi-Marín, D.M. Többens, A. Rivera-Calzada and C. León, *Solid State Ion.* **266**, 2014, 1–8.

[24]

H. Aono, E. Sugimoto, Y. Sadaoka, N. Imanaka and G. Adachi, *Chem. Lett.* **19**, 1990, 1825–1828.

[25]

S. Wong, P.J. Newman, A.S. Best, K.N. Nairn, D.R. MacFarlane and M. Forsyth, *J. Mater. Chem.* **8**, 1998, 2199–2203.

[26]

J. Wolfenstine, D. Foster, J. Read and J.L. Allen, *J. Power Sources* **182**, 2008, 626–629.

[27]

J. Wolfenstine, J.L. Allen, J. Summer and J. Sakamoto, *Solid State Ion.* **180**, 2009, 961–967.

[28]

Z.A. Munir, U. Anselmi-Tamburini and M. Ohyanagi, *J. Mater. Sci.* **41**, 2006, 763–777.

[29]

W.D. Kingerg and H.K. Bowen, Introduction to Ceramics, (Chapter 10)1976, Wiley-Interscience publications; New York.

[30]

M. Nygren, *J. Iron Steel Res.* **14**, 2007, 99–103.

[31]

G. Delaizir, V. Viallet, A. Aboulaich, R. Bouchet, L. Tortet, V. Seznec, M. Morcrette, J.M. Tarascon, P. Rozier and M. Dollé, *Adv. Funct. Mat.* **22**, 2012, 2140–2147.

[32]

T. Takeuchi, H. Kageyama, K. Nakanishi, M. Tabuvhi, H. Sakaebe, T. Ohta, H. Senoh, T. Sakai and K. Tatsumi, *J. Electrochem. Soc.* **157**, 2010, A1196–A1201.

[33]

Y. Kobayashi, H. Miyashiro, T. Takeuchi, H. Shigemura, N. Balakrishnan, M. Tabuchi, H. Kageyama and T. Iwahori, *Solid state Ion.* **152–53**, 2002, 137–142.

[34]

R. Kali and A. Mukhopadhyay, *J. Power Sources* **247**, 2014, 920–931.

[35]

R. Kali and A. Mukhopadhyay, *J. Power Sources* **247**, 2014, 920–931.

[36]

Y. Kobayashi, T. Takeuchi, M. Tabuchi, K. Ado and H. Kageyama, *J. Power Sources* **81–82**, 1999, 853–858.

[37]

C.M. Chang, Y.I. Lee, S.H. Hong and H.M. Park, *J. Am. Ceram. Soc.* **88**, 2005, 1803–1807.

[38]

Z. Wen, X. Xu and J. Li, *J. Electroceram.* **22**, 2009, 342–345.

[39]

X. Xu, Z. Wen, X. Yang and L. Chen, *Mat. Res. Bull.* **43**, 2008, 2334–2341.

[40]

S. Duluard, A. Paillassa, L. Puech, P. Vinatier, V. Turq, P. Rozier, P. Lenormand, P. Taberna, P. Simon and F. Ansarta, *J. Eur. Ceram. Soc.* **33**, 2013, 1145–1153.

[41]

J.S. Lee, C.M. Chang, Y.I. Lee, J.H. Lee and S.H. Hong, *J. Am. Ceram. Soc.* **87**, 2004, 305–307.

[42]

C. Chang, S. Hong and H. Park, *Solid State Ion.* **176**, 2005, 2583–2587.

[43]

M. Pérez-Estébanez, J. Isasi-Marín, C. Díaz-Guerra, A. Rivera-Calzada, C. León and J. Santamaría, *Solid State Ion.* **241**, 2013, 36–45.

[44]

M. Nygren and Z. Shen, Ceramic Science and Technology, *Hot Pressing and Spark Plasma Sintering* **vol. 3**, 2012, Willey-VHC; Germany, 189–214.

[45]

J. Rodríguez-Carvajal, "FULLPROF: A Program for Rietveld Refinement and Pattern Matching Analysis", Abstracts of the Satellite Meeting on Powder Diffraction of the XV Congress of the IUCr, 1990, 127, Toulouse, France.

[46]

F. Lange, *J. Am. Ceram. Soc.* **72**, 1989, 3–15.

[47]

H. Aono, Studies on Li^+ Ionic Conducting Solid Electrolyte Composed of Nasicon-type Structure, PhD thesis1994.

[48]

P. Scherrer, *Mathematisch-Physikalische Kl.* **2**, 1918, 98–100.

[49]

M. Suarez, J.L. Menéndez and R. Torrecillas, *Scr. Mater.* **61**, 2009, 931–934.

[50]

K. Arbi, R. Jimenez, T. Šalkus, A.F. Orliukas and J. Sanz, *Solid State Ion.* **271**, 2014, 28–33.

[51]

K. Arbi, W. Bucheli, R. Jiménez and J. Sanz, *J. Eur. Ceram. Soc.* **32**, 2015, 1477–1484.

[52]

P. Zhang, M. Matsui, Y. Takeda, O. Yamamoto and N. Imanishi, *Solid State Ion.* **263**, 2014, 27–32.

[53]

P. Zhang, H. Wang, Q. Si, M. Matsui, Y. Takeda, O. Yamamoto and N. Imanishi, *Solid State Ion.* **272**, 2015, 101–106.

[54]

X. Xu, Z. Wen, J. Wu and X. Yang, *Solid State Ion.* **178**, 2007, 29–34.

[55]

C. Guizard, S. Surbé, G. Baldinozzi and A. Addad, *Acta Mater.* **56**, 2008, 4658–4672.

Graphical abstract

elsevier_JALCOM_35121

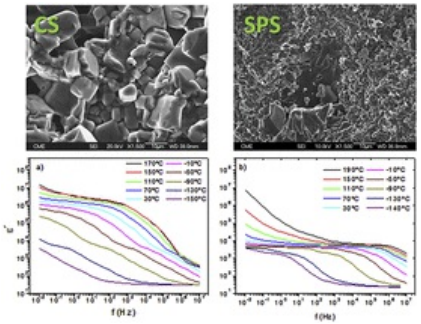

Highlights

- SPS allows complete densification of $Li_{1+x}M_xTi_{2-x}(PO_4)_3$ powders.
- Optimal sintering conditions to avoid grain growth are stated.
- The activation energies of dc and grain boundary conductivity are independent of the density.
- Pre-exponential factors are responsible for changes in conductivity with density.
- The use of SPS produces electrically well-defined grain boundaries.

Queries and Answers

Query: Please check the address for the corresponding author that has been added here, and correct if necessary.
Answer: It's correct

Query: Please note that author's telephone/fax numbers are not published in Journal articles due to the fact that articles are available online and in print for many years, whereas telephone/fax numbers are changeable and therefore not reliable in the long term.
Answer: ok

Query: Please confirm that given names and surnames have been identified correctly.
Answer: they are ok

Query: Your article is registered as a regular item and is being processed for inclusion in a regular issue of the journal. If this is NOT correct and your article belongs to a Special Issue/Collection please contact san.natarajan@elsevier.com immediately prior to returning your corrections.
Answer: Yes